Terra Antartica
1998, **5**(3), 383-391

Laser-Derived Particle Size Characterisation of CRP-1, McMurdo Sound, Antarctica

K.J. WOOLFE[1], C.R. FIELDING[2], J.A. HOWE[3], M. LAVELLE[3] & J.H. LALLY[1*]

[1]School of Earth Sciences, James Cook University, Townsville, Qld 4811 - Australia
[2]Department of Earth Sciences, University of Queensland, Qld 4072 - Australia
[3]British Antarctic Survey, High Cross, Madingley Road, Cambridge CB3 0ET - United Kingdom
[*]Current address: SRK Consulting, PO Box 943, West Perth, WA 6872 - Australia

Received 26 July 1998; *accepted in revised form* 15 October 1998

Abstract - Laser-derived particle size determinations of gravel-free samples obtained at *c.* 1 m intervals through out the CRP-1 core are presented. These data were collected using a Malvern Mastersizer-X long bed instrument and are presented as unmodified laser diffraction diameters. Eight broad textural zones are identified. The bulk of samples show a moderate degree of sorting indicating that little if any ice-contact sedimentation is preserved with in the cored interval. A regular variation in mode and median particle size occurs approximately every five metres throughout much of the core and is suggestive of environmental forcing.

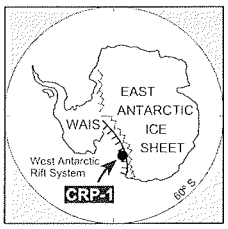

INTRODUCTION

The stratigraphic drill hole CRP-1 was drilled to a depth of 147 mbsf, in McMurdo Sound during October 1997 as part of the International Cape Roberts Project. The hole intersected a 43.15 m-thick early Quaternary glacimarine sequence (Cape Roberts Science Team, 1998; Fielding et al., this volume (Sequence Stratigraphic Analysis of CRP-1)). This succession unconformably overlies glacimarine strata of early Miocene age (Cape Roberts Science Team, 1998) in which the hole was terminated. CRP-1 is the latest in a series of holes drilled to investigate the Cenozoic evolution of the Ross Embayment and adjacent East Antarctic ice sheet (Pyne et al., 1985; Barrett, 1986, 1989, 1996; Robinson et al., 1987).

In this paper we present the results of a laser-diffraction particle size characterisation of the CRP-1 drillcore. The study was conducted to examine metre-scale textural variability within the core as a aid to palaeoenvironmental interpretation and to provide base-line data for geochemical and physical property studies.

Laser diffraction was chosen in preference to other sizing methods due largely to its rapidity and the reproducibility of the results (see below). The data are presented as uncorrected laser diffraction diameters and the authors recognise that these may not be directly comparable with data derived from sieve-sedigraph or settling tube experiments. These differences arise in part from shape functions which are sample-dependent, and in part from different instrumental methodologies for dealing with particles falling close to the fine-grained detection limit. Other discrepancies (especially in fine-grained particles) are likely to stem from slightly different sample preparation procedures, together with the temperature, ionic strength and concentration of the suspension. Despite these differences in detail, it should be noted that the internal reproducibility of results from laser diffraction is excellent. Consequently, the method provides a fast and reliable mechanism, for detecting textural trends. Comparable laser diffraction data from nearby stratigraphic drillholes (CIROS-1, CIROS-2 and MSSTS-1) are currently being assembled.

METHODOLOGY

Samples of approximately 1 cm^3 were collected at *c.* 1 m spacing throughout the length of CRP-1. Samples were tested for carbonate using 10% HNO_3, and where carbonate was detected the samples were digested in excess acid until effervescence ceased. The acid-treated samples were then washed prior to disaggregation with the remaining sample suite. Samples were gently crushed between wooden blocks and soaked in tap water for 24 hrs or longer. Samples were optically checked for complete disaggregation. Samples which were not fully disaggregated were ultrasonically dispersed for up to 24 hrs, with the degree of disaggregation being checked periodically using a binocular microscope.

Once fully disaggregated, samples were allowed to settle and the excess supernatant fluid decanted off. After oven-drying at 60°C, samples were passed through a 2 mm sieve to remove the gravel fraction and then remixed to a thick paste (tooth paste consistency). Subsamples from the homogenised paste were resuspended in *c.* 1 litre of tap water and ultrasonically dispersed. Sufficient sample was added to achieve a laser obscuration of between 5 and 15% over a 2.5 mm transmission path length (for most lithologies this required about 0.5 g of sample).

Size determinations were obtained using a Malvern Mastersizer-X, long bed, laser diffraction particle sizer. The instrument uses conventional Fourier optics to analyse

the particle-induced scattering (diffraction) of an 18 mm diameter red (590 nm, Helium-Neon) laser beam as it intersects suspended particles in the sample chamber.

Essentially, the diameters of all particles entrained in an upward-directed turbulent flow are determined in a single diffraction observation. Fifteen thousand observations were obtained for each sample and the reported results represent an average of these observations. The scattered laser light is collected on 32 detectors, giving in this case (using a 1 000 mm lens), 32 size bins between 4 µm and 2 000 µm. Volumetric distributions were then determined using a polydisperse model. The data were then exported to Excel using a modified version of Woolfe & Michibayashi's (1995) dynamic data exchange (DDE) link.

The instrument was routinely checked against a glass bead standard to assess analytical errors (Fig. 1). Subsample variability was estimated by triplicate runs of selected samples and in all cases sub-sample variability exceeds instrumental error (Fig. 2).

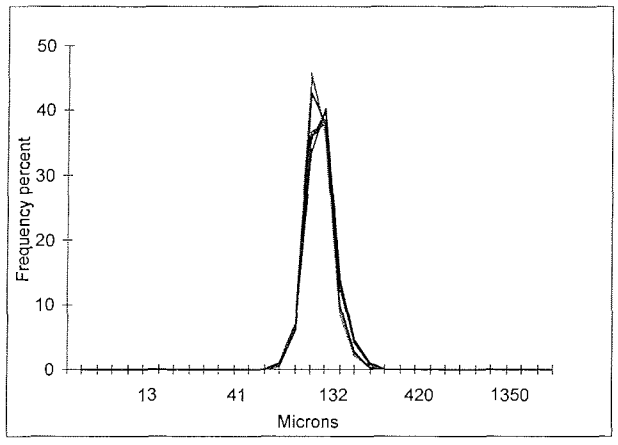

Fig. 1 - A 90-95 µm glass bead standard was analysed between every 10-15 Cape Roberts samples as an internal check on calibration. The data presented here represent all of the glass bead experiments, and are presented without modification. They illustrate the internal consistency of the methodology: the ten experiments yield a mean of 93.96 µm, and a standard deviation of 1.80 µm.

Many of the samples are polymodal (Appendix 1); therefore conventional distribution measures such as distribution mean, standard deviation and skewness are not entirely appropriate as they describe variability about an idealised normal distribution. Consequently, we have also chosen to characterise the particle size distribution using primary mode (M1), 25th percentile (d25), median (d50) and a derived parameter approximating polymodal skewness (d50-M1). While these parameters do not fully describe the entire particle size spectra, they serve as a reasonable proxy, although limitations clearly apply. Further characterisation of the core was attempted using Entropy analysis.

Entropy analysis groups frequency data without assuming any predetermined distribution. Consequently, the method is well suited to the analysis of polymodal particle size data. A number of authors have applied the technique to a variety of geographical (Semple & Golledge, 1970; Semple et al., 1972; Johnston, 1978; Thomas, 1981; Johnston & Semple, 1983) and geological applications (Sharp, 1973; Sharp & Fan, 1973; Ehrlich, 1983; Full et al., 1983; Forrest & Clark, 1989; Woolfe & Michibayashi, 1995; Woolfe, 1995). The groupings presented here were obtained using ENTROPY4, a modified version of Woolfe & Michibayashi's (1995) Quickbasic program. However, the fundamental methodology is largely unaltered from Semple et al.'s (1972) multivariate extension to information theory.

Effectively, ENTROPY4 groups samples in much the same way as one would group them by eye using histograms. The total inequality, or regularity statistic [I(Y)] for all the samples in the data set is calculated as

$$I(Y) = \sum_{j=1}^{J} Y_j \sum_{i=1}^{N} Y_i \log_2 N Y_i$$

where: Yj = frequency value (of particles) in class j; J=number of size classes; N=Number of samples (rows);

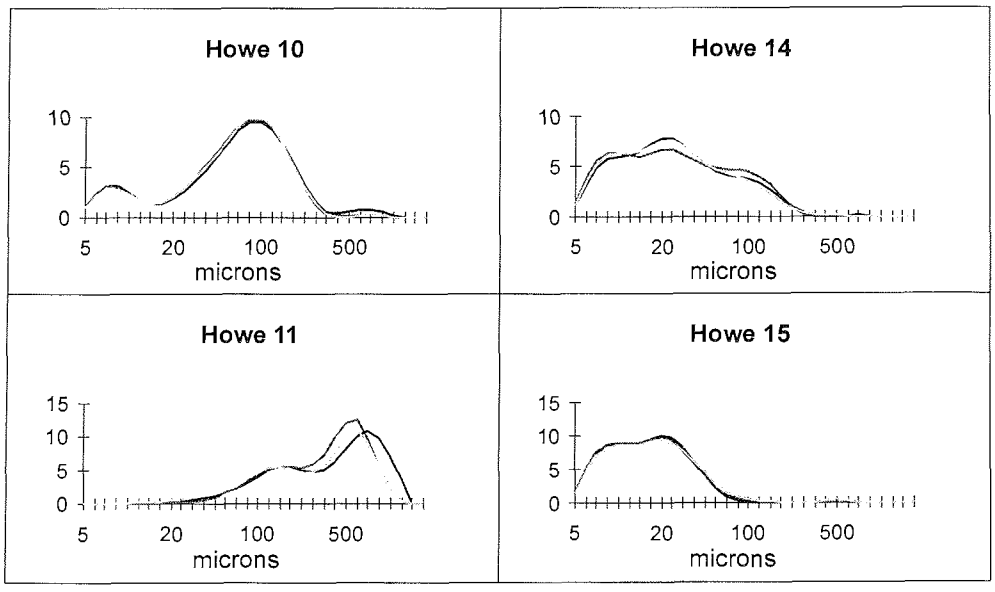

Fig. 2 - Additional particle size samples were collected to charcterise possible gravity flows (see Howe et al., this volume). These samples were run in triplicate to investigate within-sample variability. The primary causes of variability within samples is hydraulic sorting during subsampling. These four examples illustrate the magnitude of experimental error that might be expected within the CRP-1 sample suite.

Yi = frequency value (of particles) in class j that are sample i, such that Yi=Yij/Yj; Yij = proportion of the total population (all of K samples) in row i, column j. Then

$$\sum_{j=1}^{J} Y_j = 1.0 \quad \text{and} \quad \sum_{i=1}^{K} Y_i = 1.0$$

The I(Y) statistic is a measure of the inequality in the distribution of class values over all the samples, weighted by the frequency of particles within each class.

The user selects a number of groups into which the samples will be divided, in this case all combinations for 2 to 12 groups were calculated. The samples are initially divided equally between the groups, so that if ten samples [N] are input and five groups [R] selected, samples 1 and 2 will be allocated to group 1, samples 3 and 4 to group 2, and so on. Starting with this arbitrary allocation of samples to groups, the between-group inequality is calculated, using the formula

$$I_B(Y) = \sum_{j=1}^{J} Y_j \sum_{r=1}^{R} Y_{jr} \log_2 \frac{Y_{jr}}{N_r / N}$$

where R = total number of groups (r) and $I_B(Y)$ = between group inequality.

The process is repeated so that all possible configurations of N samples into R groups are considered. The aim is to find the optimal classification of samples into groups so that the within-group inequality is minimised and the between-group inequality maximised. This is measured by dividing the between-group inequality for a particular configuration by the total inequality (the result is called the R_S statistic); the closer this value is to one, the more the data set can be 'explained' by the grouping. The statistical optimal number of groups for a data set is actually the point at which the R_S statistic begins to increase at a significantly slower rate with an increasing number of groups, since the 'best' grouping in these terms would be when R = N (*i.e.* when each sample is placed in its own group).

A particularly useful aspect of entropy analysis is that any number of groups (from 1 to the number of samples) can be achieved. Regardless of the number of groups selected, the data are sorted so that similar samples are classed together.

RESULTS

Individual particle size distributions for all samples analysed are shown in appendix 1.

The relative proportions of sand, silt and clay were determined such that reported clay represents particles with laser diffraction diameters of 12 μm and less. This is considerably coarser than the traditional clay-silt boundary. However, we have chosen 12 microns, because laser diffraction diameters of fine-grained particles are typically larger than the equivalent diameters determined by settling or SediGraph, and because it can be shown experimentally that most mineral particles finer than 12 μm (laser diffraction diameter) behave electrostatically, *i.e.* are hydrodynamically and electrochemically clay-like (new data). The sand-silt boundary was retained at 63 μm.

Systematic down-hole changes in the relative proportions of sand, silt and clay are not strongly evident (Fig. 3a). Smoothing the data (3 sample rolling average, Fig. 3b) reveals several weakly developed coarsening upwards megacycles. A series of smaller scale cycles are superimposed on top of these. However, the systematic cyclicity evident in CIROS-1 (Fielding et al., 1997) is not so well developed in CRP-1. Moreover abrupt changes in the sand/silt/clay ratios do not closely correspond with identified sequence boundaries. Instead, variability appears to be dominated by small-scale facies changes which typically occur every 5 m or so throughout the core.

Down-hole variability in modal particle size (M1, Fig. 4) is dominated by a series of coarse-grained intervals in the lower half of the hole. These sandy intervals have median grain-sizes in excess of 500 μm. No large-scale trends are evident in the data. With the exception of a sand-dominated interval between 56 mbsf and 68 mbsf, the core is characterised by a silt-sized mode which is interrupted by sandy pulses, many of which may represent single

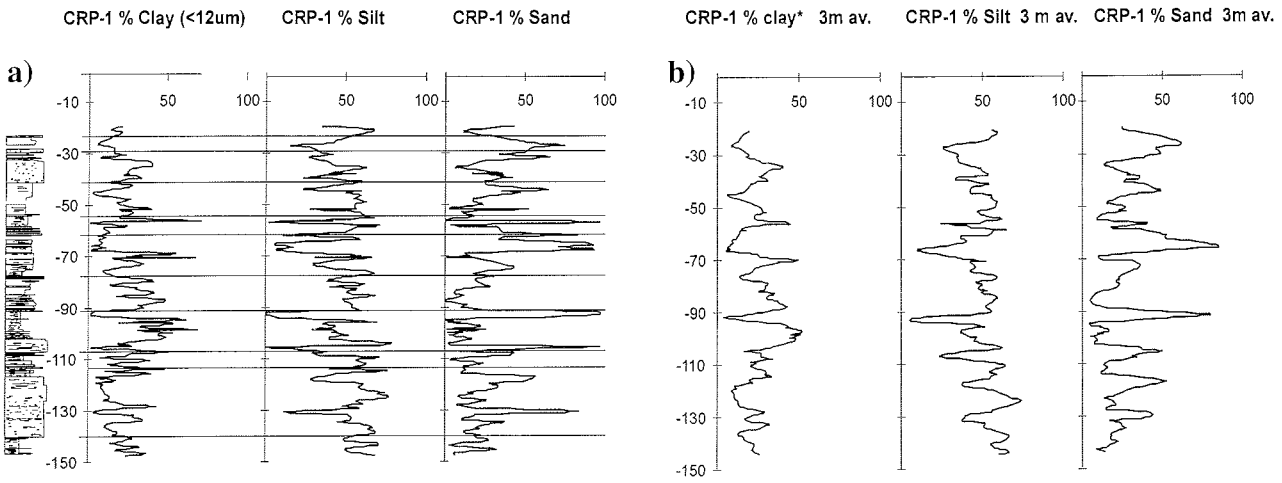

Fig. 3 - Down-hole variability of sand, silt and clay using both individual samples (*a*) and smoothed using a 3-point running average (*b*). Horizontal solid lines mark sequence boundaries from Fielding et al. (see Sequence Stratigraphic Analysis of CRP-1, this volume).

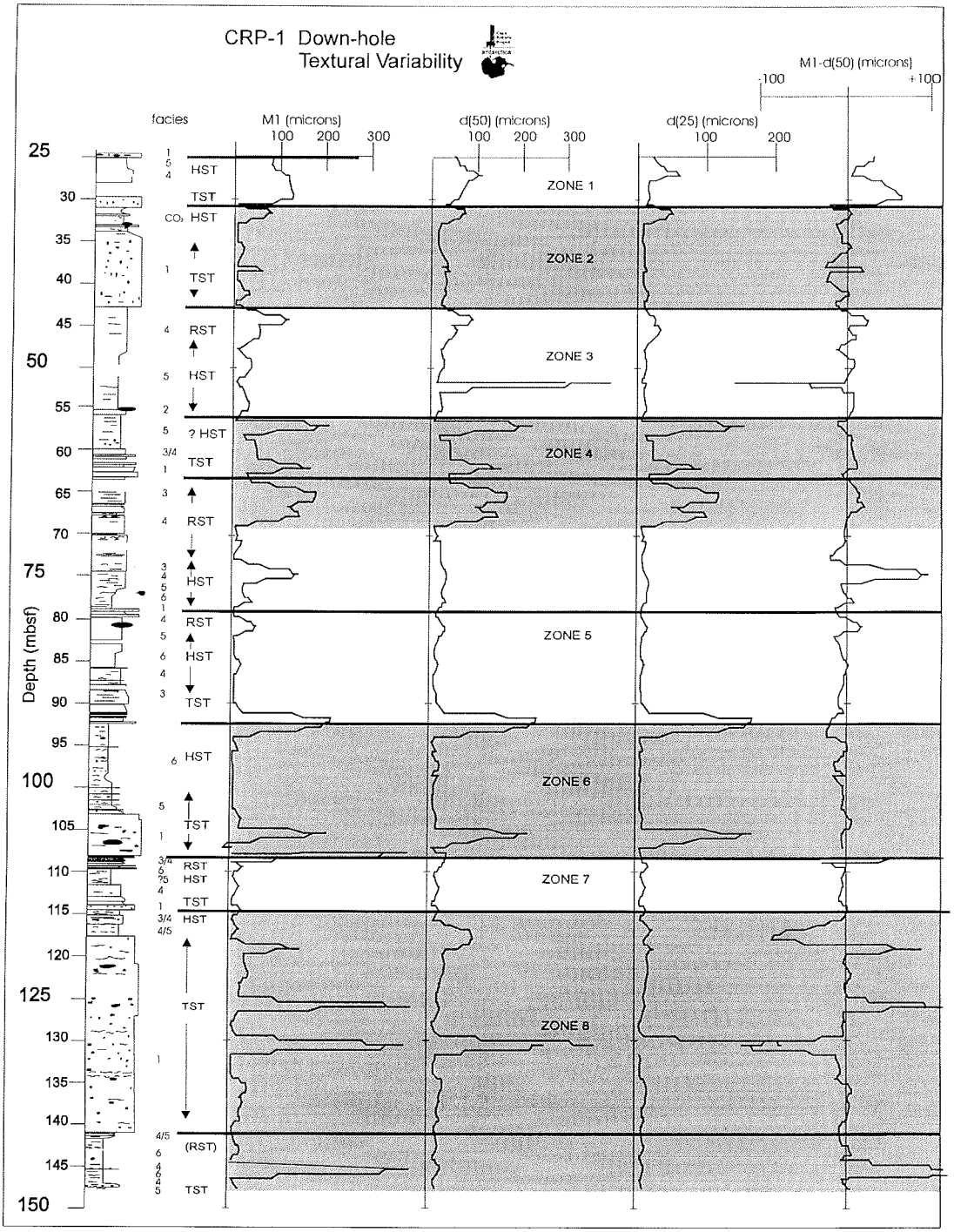

Fig. 4 - Down-hole variability in primary mode (M1), median (d50), 25th coarsening percentile (d25) and a derived skewness/bimodality parameter (M1-d50). Eight meso-scale textural zones are delineated and are here plotted against lithostratigraphy and sequence stratigraphy (horizontal solid lines mark sequence boundaries) from Fielding et al. (see Sequence Stratigraphic Analysis of CRP-1, this volume).

events. Similar trends are evident in the median and 25th percentile diameters (d(50), d(25), Fig. 4).

The bimodality/skewness proxy (M1-d50, Fig. 4) provides measure deviation from a normal distribution. For a unimodal normal distribution M1-d50 is zero, the addition of a coarse-grained mode produces a positive excursion, whereas the addition of a fine-grained mode generates negative excursions. As with the other textural variables down-hole trends are dominated by sandy intervals and show little direct correlation to the sequence stratigraphic boundaries identified by Fielding et al. (this volume).

By considering M1, d(50), d(25) and the skewness proxy, eight broad textural zones can be identified (Fig. 4). Zone 1 (0-32 mbsf) is restricted to cycle 10 (Cape Roberts Science Team,1998) and is defined by a coarser primary mode (M1 = *c.* 100 um) and median (d(50) = *c.* 75 um) and a positive skewness proxy. Zone 2 (32-43 mbsf) is restricted to the lower of the two Quaternary cycles (cycle 9) and is defined by minimal variation in mode, median and 25th percentile and a largely negative skewness proxy. Zone 3 (43-56 mbsf) is restricted to the youngest Miocene cycle (cycle 8) and is characterised by a weak coarsening upwards cycle with three small coarsening cycles

superimposed on a 3-5 metre scale. These are best depicted by variations in the primary mode although coarsening is also evident in d(50) and d(25). Zone 4 (56-68 mbsf) includes all of cycle 7 and the upper portion of cycle 6. This zone is markedly coarser grained, and demonstrates apparent internal variability on a *c.* 5 metre-scale. Zone 5 (68-92 mbsf) includes the lower half of cycle 6 and all of cycle 5. The zone is characterised by 5 metre-scale variability in primary mode and to a lesser extent concordant variability in d(50), d(25) and the skewness proxy. With the exception of a coarse-grained interval at its base, the zone displays a weakly developed coarsening upwards trend which extends into zone 4. Zone 6 (92-108 mbsf) is restricted to cycle 4 and is characterised by relatively little variation in mode, median and 25th percentile. Zone 6 is the only interval in which a *c.* 3-5 metre-scale variability in particle size is not developed. Zone 7 (108-114 mbsf) is a fine-grained interval, with a negative skewness proxy and *c.* 3 metre-scale variability in primary mode, median and 25th percentile. The zone is restricted to cycle 3. Zone 8 (114-147 mbsf) includes all of cycle 1 and 2. The interval is characterised by 5 metre-scale variability in mode and median with superimposed sandy spikes and strong positive and negative excursion in skewness proxy.

The data group moderately well using Entropy analysis, with the statistical optimum number of groups being four (Fig. 5). These entropy facies are sumarised in figure 6 and consist of a very poorly sorted silty sand (Group 1), a moderately sorted medium sand (Group 2), a poorly sorted sandy silt (Group 3) and a moderately sorted coarse sand (Group 4). Down-hole variability in Entropy facies (Fig. 7) reveals facies dislocations at many of the sequence boundaries. Group 1 sediments are dominant in the upper and lower portions of the hole (cycles 2-3 and 6-10), whereas Group 3 sediments are dominant in cycles 3-5.

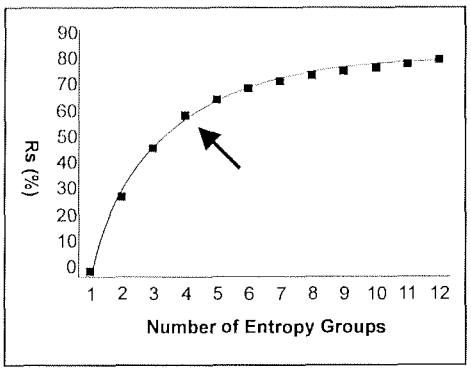

Fig. 5 - Plot of Rs statistic verses number of entropy groups for the CRP-1 samples. The statistical optima occurs at n=4 (arrowed).

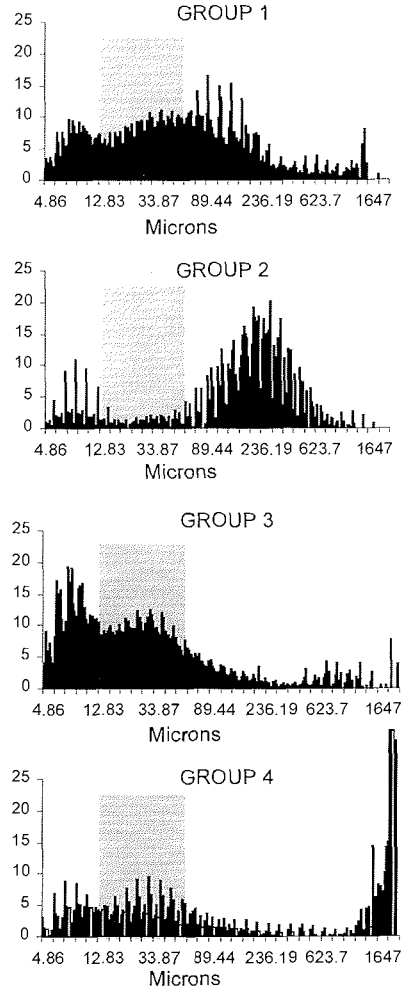

Fig. 6 - Particle size distributions of the four entropy groups selected. Shaded area is silt (see text for discussion).

DISCUSSION AND CONCLUSIONS

Large-scale down-hole variability in textural parameters, such as that exhibited in CIROS-1 (Fielding et al., 1997), is not strongly evident in CRP-1. Suggesting that major changes in textural environment did not occur during the cored interval. However, at a detailed level, there is significant variability between samples. Many of the samples have moderately to well-sorted modes suggestive of subaqueous transport and deposition. Only a very few samples appear as true admixtures such as might be expected from ice-contact deposition (see De Santis & Barrett, this volume). There is a marked change in the character of the core at *c.* 70 m. Above 70 m (textural zones 1-4), the core is characterised by sandy sediments with broad textural excursions. However, below 70 m the core is characterised by fine-grained sedimentation that is punctuated by coarse-grained sandy spikes. Many of these spikes are inferred to have been produced by gravity flows (see Howe et al., this volume).

A regular variation in modal and median particle size occurs throughout most of the core over three to five metre intervals This variation is suggestive of cyclic processes affecting the depositional environment. Correlation with the well dated Miocene section of CRP-1 (44 mbsf to 117 mbsf in Lavelle, this volume) suggests gross particle size variations may have been tuned to the 100 k.y. eccentricity signal (fifteen 5 m cycles deposited over ~75 m in ~1.5 m.y.). The absence of large-scale trends and strong dislocations in the data suggests that similar processes acted through the period of deposition and that facies changes may reflect only minor changes in overall environment.

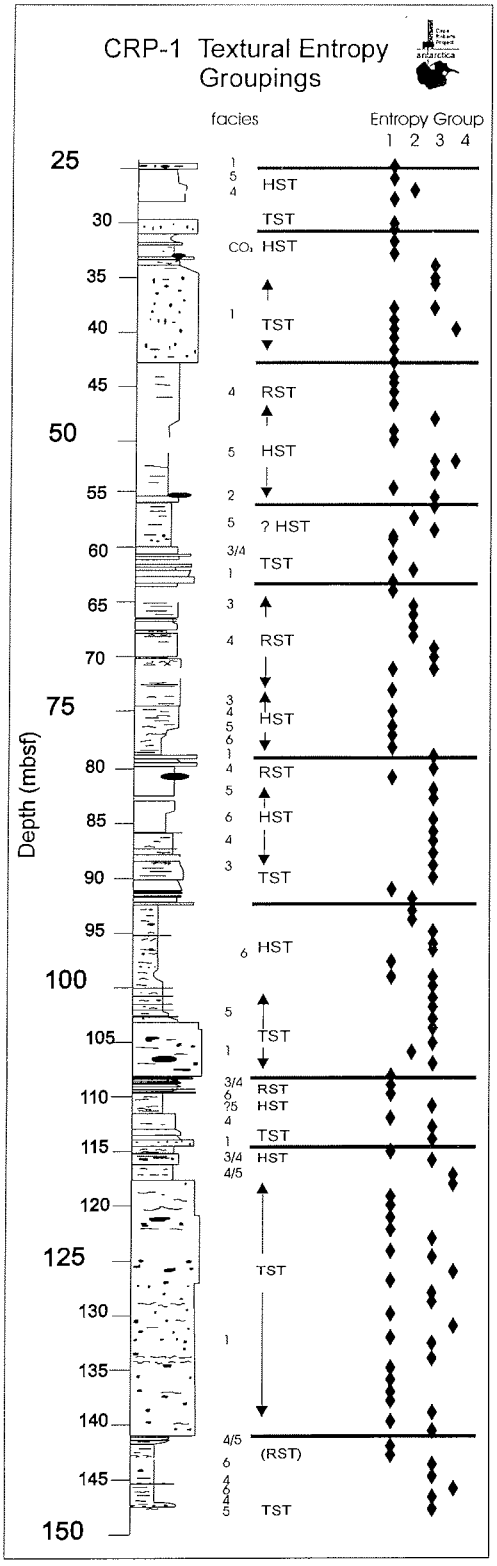

Fig. 7 - Down-hole variability in entropy group. Sequence boundaries (bold lines) and stratigraphy from Fielding et al. (see Sequence Stratigraphic Analysis of CRP-1, this volume).

Eight textural zones are defined and these broadly agree with the sequence stratigraphic boundaries defined by Fielding et al. (see Sequence Stratigraphic Analysis of CRP-1, this volume). An exception to this is a marked textural change in the core at the base of textural zone 4. This textural boundary occurs in the middle of sequence stratigraphic cycle 6, however, the corresponding change from silty sand (Group 1) to sandy silt (Group 3) does not occur until the sequence boundary at the base of cycle 6. Suggesting that the cycle 5 sequence boundary may be misplaced or that an additional sequence boundary may be called for at *c.* 70 mbsf.

Four entropy facies are defined. Two muddy facies. (Groups 1 and 3) reflect varying proportions of sand and silt. A moderately sorted medium sand (Group 2) occurs at several intervals through out the core and probably represents current reworking of adjacent glacimarine (group 1 and 3) sediment. Whereas the slightly muddy coarse sand (Group 4) is largely restricted to the lower portion of the hole where it is the inferred product of gravity flow processes (Howe et al., this volume).

ACKNOWLEDGEMENTS

This paper was made possible through the collective efforts of the International Cape Robert Project and the authors express their gratitude to the entire project team. Daniel McNamara and Chris Weigt assisted with sample preparation and laser diffraction observations were conducted in the Environmental Sedimentology Laboratory at JCU. This work was jointly funding by the Australian Research Council and James Cook University.

REFERENCES

Barrett P.J. (ed.), 1986. Antarctic Cenozoic history from the MSSTS-1 drillhole, McMurdo Sound. *DSIR New Zealand Bulletin*, **237**, 174 p.

Barrett P.J. (ed.), 1989. Antarctic Cenozoic history from the CIROS-1 drillhole, McMurdo Sound. *DSIR New Zealand Bulletin*, **245**, 254 p.

Barrett P.J., 1996. Antarctic PalaeoEnvironment through Cenozoic Times - A Review. *Terra Antartica*, **3**, 103-119.

Cape Roberts Science Team, 1998. Initial Report on CRP-1, Cape Roberts Project, Antarctica. *Terra Antartica*, **5**(1), 187 p.

Ehrlich R., 1983. Size analysis wears no clothes, or have moments come and gone? *Jour. Sedim. Petrology*, **53**, 1.

Fielding C.R., Woolfe K.J., Purdon R.G., Howe J.A & Lavelle M., 1997. Sedimentological and Sequence Stratigraphic Re-Evaluation of the CIROS-1 Core, McMurdo Sound, Antarctica. *Terra Antartica*, **4**(2), 149-160.

Forrest J. & Clark N.R., 1989. Characterising grain size distributions: evaluation of a new approach using a multivariate extension of entropy analysis. *Sedimentology*, **36**, 711-722.

Full W.E., Ehrlich R. & Kennedy S.K., 1983. Optimal definition of class intervals for frequency tables. *Particulate Science and Technology*, **1**, 281-293.

Johnston R.J., 1978. *Multivariate statistical analysis in geography: a primer on the general linear model*. Longman, London, 280 p.

Johnston R.J. & Semple R.K., 1983. Classification using information statistics. *Concepts and Techniques in Modern Geography*, **37**, 38 p.

Pyne A.R., Robinson P.H. & Barrett P.J., 1985. Core log, description and photographs - CIROS-2 - Ferrar Fjord, Antarctica. Victoria University of Wellington, *Antarctic Data Series*, **11**, 80 p.

Robinson P.H., Pyne A.R., Hambrey M.J., Hall K.J. & Barrett P.J., 1987. Core log, photographs and grain size analyses from the CIROS-1 drillhole, western McMurdo Sound, Antarctica. Victoria University of Wellington, *Antarctic Data Series*, **14**, 241 p.

Semple R.K. & Golledge R.G., 1970. An aualysis of entropy changes in a settlemeut pattern over time. *Economic Geography*, **46**, 157-160.

Semple R.K., Youngman C.E. & Zeller R.E., 1972. *Economic Regionalization and information theory; An example*. Discussion Paper 28, Dpt. of Geography, Ohio State Univ. Columbus, 64 p.

Sharp W.E., 1973. Entropy as a parity check. *Earth Research*, **1**, 27-30.

Sharp W.E. & Fan P., 1963. A sorting Index. *Journal of Geology*, **71**, 76-84.

Thomas R.W., 1981. Information statistics in Geography. *Concepts and Techniques in Modern Geography*, **31**,1-40.

Woolfe K.J., 1995. Textural entropy groupings from a modern lake-lagoon system and its ancient aualogue. *New Zealand Journal of Geology and Geophysics*, **38**, 259-262.

Woolfe K.J. & Michibayashi K., 1995. BASIC entropy grouping of laser-derived grainsize data: an example from the Great Barrier Reef. *Computers and Geosciences*, **21**, 447-462.

Appendix 1 - Laser diffraction particle size distributions for all samples. Shaded area denotes silt-grade material. Graph titles are sample depth in mbsf.

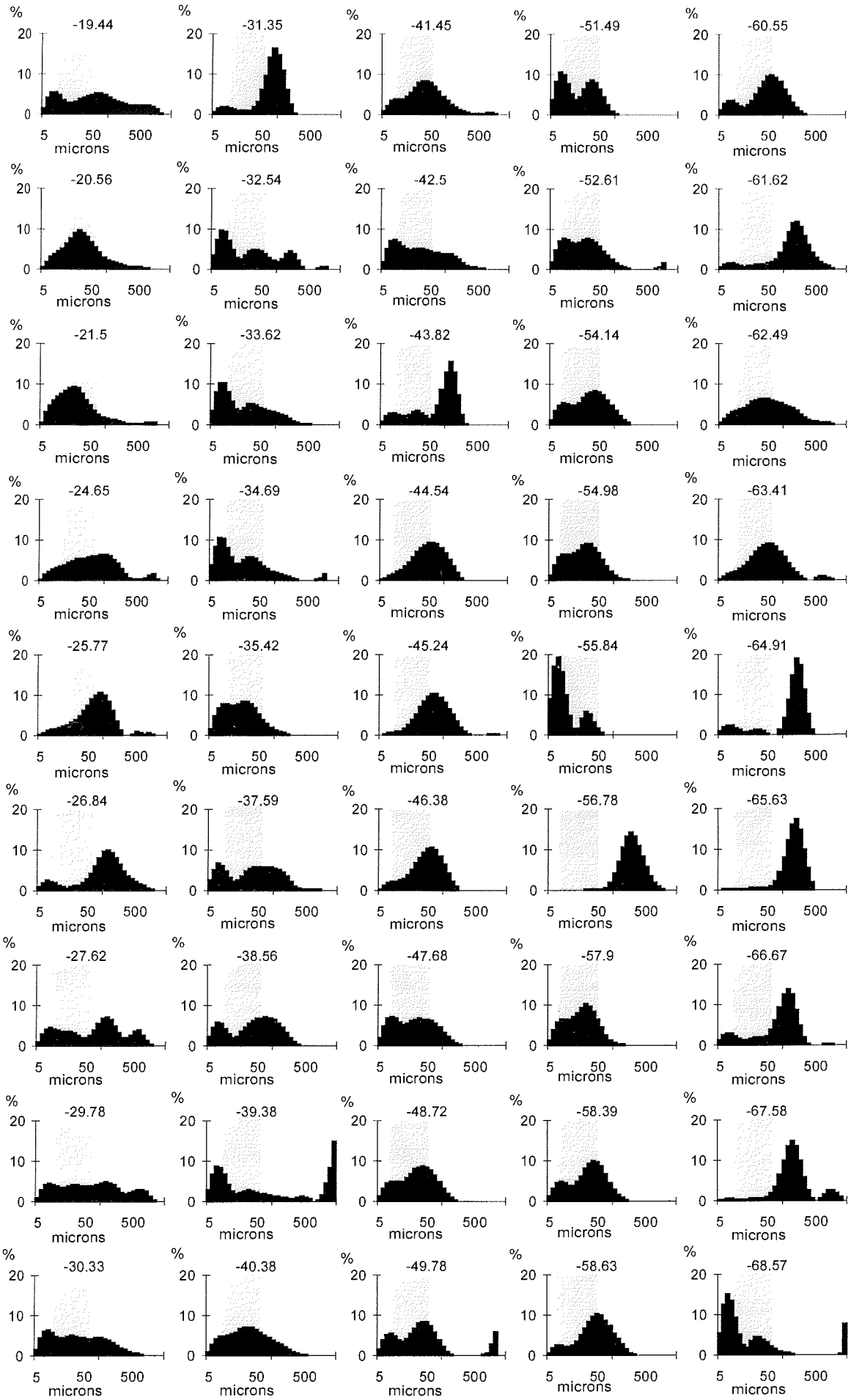

Appendix 1 - Continued.

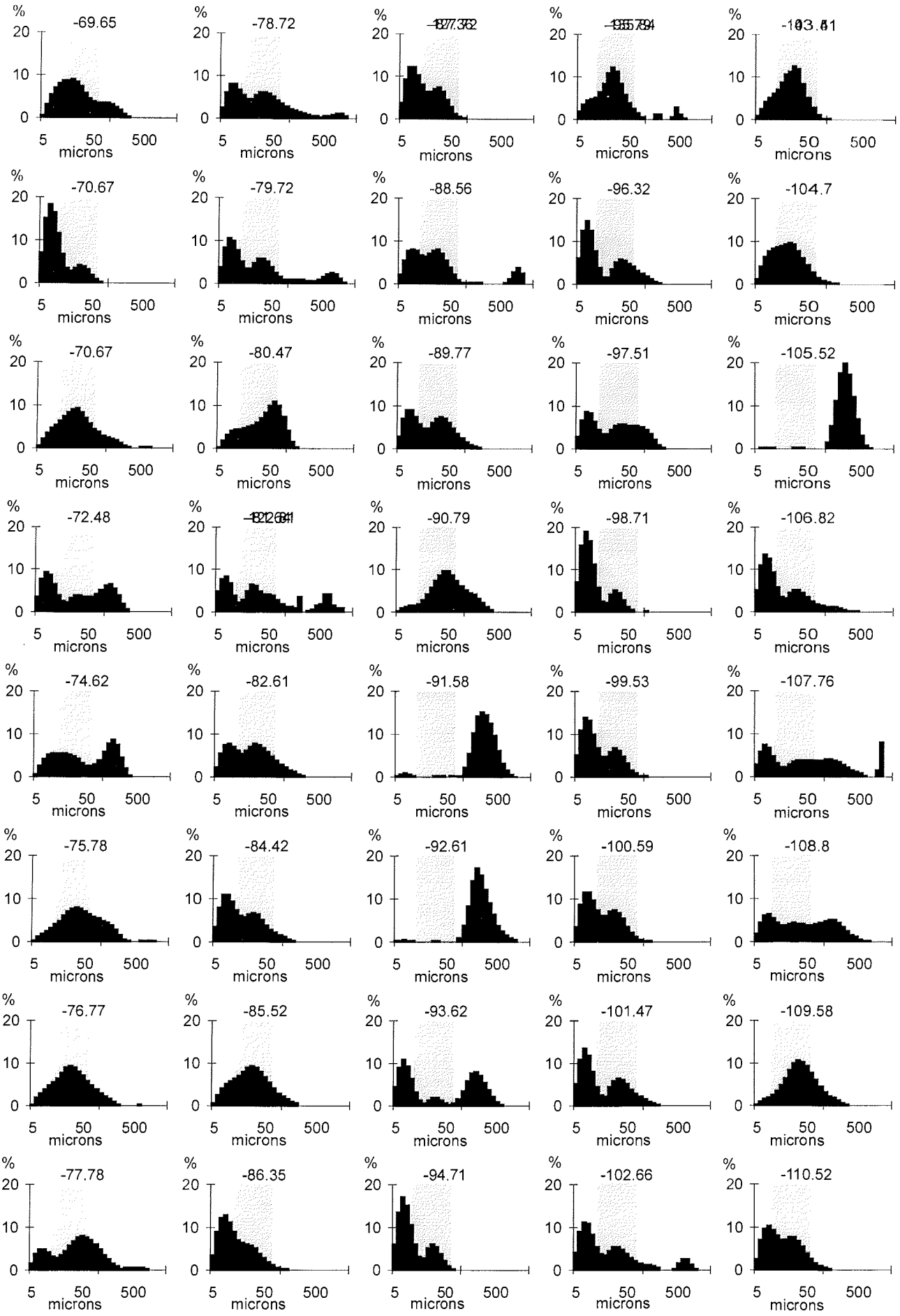

Appendix 1 - Continued.